Analysis of an innovative design for an axial flux Torus machine

M. Cirani, C. Sadarangani and P. Thelin

Division of Electrical Machines and Power Electronics, Royal Institute of Technology
Teknikringen 33, 100 44 Stockholm, Sweden
phone: +46 8 790 90 38 – fax: +46 8 20 52 68 - e-mail: peter.thelin@ekc.kth.se

***Abstract* — This paper presents an innovative design of a 30 kW, 4000 r/min axial-flux permanent magnet Torus machine to be integrated in a hybrid electric vehicle. To this end the Torus machine must be designed for traction applications. To fulfill the requirements of high speed, the stator of the machine is provided with stator teeth to improve the machine field weakening capability. Finite Element calculations were performed and the results are presented here. A prototype of the machine has been manufactured and the measurements present satisfactory agreement with the analytical calculations.**

1. Introduction

Many factors point to the need to improve air quality, especially in areas with high traffic density, to protect the environment and to reduce oil consumption [1], [2]. The introduction of electric and hybrid vehicles would be beneficial in this respect. However, light-duty pure electric vehicles are not yet competitive in the market mainly due to the high cost, low power density and considerable recharging time of current batteries. Hybrid vehicles (HEVs), in contrast, by using the combination of the internal combustion engine (ICE) and the battery, succeed in high performance, though they do not eliminate the problem of emissions as electric vehicles do. Still, hybrids will reduce the problem of both noxious emissions and extra fuel consumption through a more limited and better use of the ICE.

A very important issue in any hybrid vehicle is the limited space available inside the vehicle. In this respect, the axial flux permanent magnet (AFPM) machines represent an optimal solution. In fact, the high compactness of AFPM machines compared with the conventional induction, DC and radial flux permanent magnet (RFPM) machines, provides a considerable reduction in volume and weight [3]. In particular, the limited axial length of AFPM machines is an important issue for HEVs. Furthermore, AFPM machines present high efficiency due to the absence of rotor currents. Different designs of airgap wound Torus machine are frequent in the literature [4], [5], [6], [7]. However, in order to be suitable for traction applications, the AFPM machine has to operate at high-torque and high-speeds. Thus, a water-cooled 30kW, 4000 r/min Torus machine has been designed to work in field-weakening operations, in order to fulfill the high-speed requirements. For this purpose, the machine stator is provided with teeth and slots so as to increase the field-weakening capability (Figure 1).

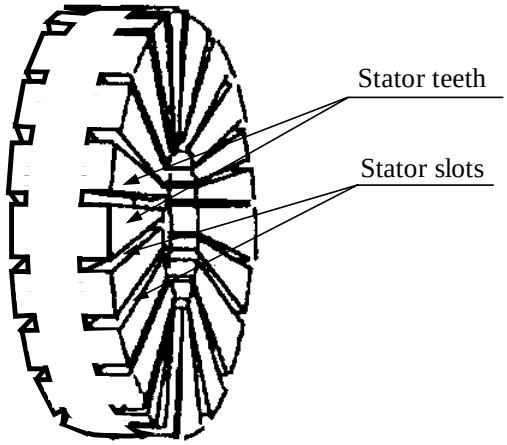

Fig 1: Torus machine with slotted stator.

A further improvement of the field-weakening capability of the machine is obtained by the addition of rotor saliency. The design of the machine presented here has been investigated on the basis of volume and performance requirements.
A general description of the machine is given. Furthermore, the performance of a machine having the previously determined parameters but without rotor saliency has been investigated and the results have been compared. FEM calculations based on the software programs Flux-2D and Flux-3D have been examined. Moreover, a simplified thermal model of the machine has been developed in order to predict the temperature rise in the winding at different operating conditions.

A prototype of the machine has been manufactured and measurements have been performed on the parameters of the prototype.

2. Components of the motor

A. Rotor

Due to the almost constant flux in the rotor, the rotor discs are made of solid iron. Rare earth magnets, in particular NeFeB magnets, have been used. Each piece of magnet has the shape shown in Figure 2. Due to the compactness of the machine, no outer bandage has been used. The rotor discs were prepared so that the saliencies could be added later by screwing steel segments of appropriate thickness onto the rotor so as to enable the study of the influence of different saliency ratios on field-weakening operation.

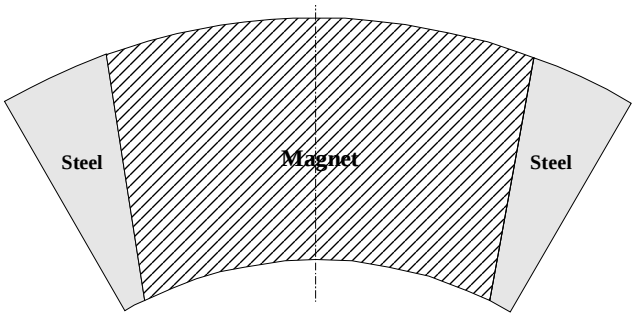

Fig.2: Magnet shape.

B. Stator

The stator of the machine is built with a sheet of laminated iron wound in a spiral fashion. The stator slots have subsequently been milled in order to create the slots. The aforesaid procedure, however, can generate problems. Due to the risk of imperfection in the iron cutting, short circuits in the iron lamination can occur. Furthermore, a non-smooth slot surface could damage the slot insulation. Thus, a further treatment must be applied on the stator back. Consequently, this is an expensive technique to manufacture the stator. As the outer surface of the stator is not perfectly circular, a layer of aluminum is placed here and machined in order to make the outer part of the stator perfectly round. This allows a perfect contact between the stator surface and the cooling case, in order to improve the machine cooling capability.

C. Stator Windings

Firstly, the slots have been covered with an insulation layer of Nomex. The windings have then been wound toroidally around the stator back. When the conductors are wound on the stator back they are distributed on the stator back surface such that the machine outer diameter is reduced as shown in Figure 3.

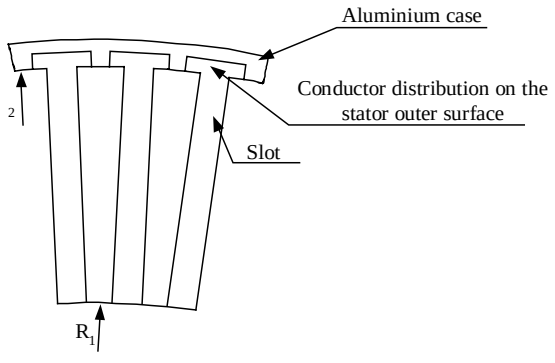

Fig. 3: Stator front section showing the conductors' distribution over the stator back.

After the windings have been set into the slot, they are impregnated with epoxy resin. Another layer of insulation then closes the slot.

D. Cooling Casing

The cooling system is an aluminum structure, which consists of two concentric rings superimposed on each other. The innermost ring is shaped so as to fit in the Torus machine outer configuration as Figure 3 shows.

Circular water channels have been machined from the outside of the inner ring. The outer ring is placed and welded over the inner ring so as to cover the water channels. Furthermore, the outside of the outer ring constitutes the machine exterior.

3. Design Analysis

The design characteristics for the Torus machine are related to the performance and volume requirements specified in Table I. For a given battery voltage, the design of the machine has been first carried out for the salient pole machine. Next, as the machine saliency is to be added later, the performance of the non-salient pole machine, based on the previously calculated parameters, has been analyzed.

TABLE I
MACHINE DESIGN REQUIREMENTS

Rated torque (T)	70 Nm
Base speed (n_b)	4000 r/min
Maximum speed (n_{max})	6000 r/min
Stator outer radius (R_2)	130 mm
Total axial length (L_T)	90 mm
Battery voltage (V_{batt})	300 V

The machine design requirements define the value of the machine output power, while the battery voltage and the converter characteristics limit the value of the input phase voltage.

TABLE II
MOTOR'S ELECTRICAL AND GEOMETRICAL CHARACTERISTICS FOR THE SALIENT POLE –MACHINE AT RATED CONDITIONS.

Peak phase voltage (U_s)	148 V
Peak phase current (I_s)	139 A
Peak current d-component (I_d)	-101 A
Peak current q-component (I_q)	95.6 A
Number of poles (p)	6
Airgap length (δ)	2 mm
Number of turns per coil	3
Magnet axial length (t_m)	3.8 mm
Peak airgap flux density (B_1)	0.65 T
Inner stator radius (R_1)	80 mm
Rotor back thickness (t_r)	13.2 mm
Stator back thickness (t_{sb})	24 mm
Total slot depth	8.2 mm
Total machine axial length (L_T)	78 mm
Maximum speed (n_{max})	6515 r/min
Inductance in the d-direction (L_d)	0.33 mH
Inductance in the q-direction (L_q)	0.89 mH

Thus, assuming an efficiency of 95% and a unitary power factor, the value of the phase current can be calculated. The parameters of the salient pole machine are reported in Table II. As the machine saliency is added later, the performance of a non-salient pole

machine with the same design parameters is analyzed in Table II. For this non-salient pole machine it was shown that, provided the total phase current is unchanged, the required torque is reached, for a higher q-component of the current. However, the machine power factor is decreased. Hence, the machine phase voltage must be increased.

4. Finite Element Analysis

A. No-load airgap flux density

The airgap flux density calculated with the 3D program in the middle of the airgap and at a radius R=105 [mm] is shown in Figure 4. As can be observed, calculations with the FEM programs produce a higher value of the airgap flux density (0.7 [T]) than the analytical calculations (0.65 [T]). This is partly due to the fact that the magnet temperature for the FEM calculation was set to 70°C, while for the analytical calculations the magnet temperature was 100°C. Analogous calculations were performed at other machine radii and the results show a higher value of the airgap flux density at the machine inner radius and a lower value at the machine outer radius compared to the center of the machine. This is due to the higher magnet-to-pole-width-ratio at the machine inner radius than at the outer one.

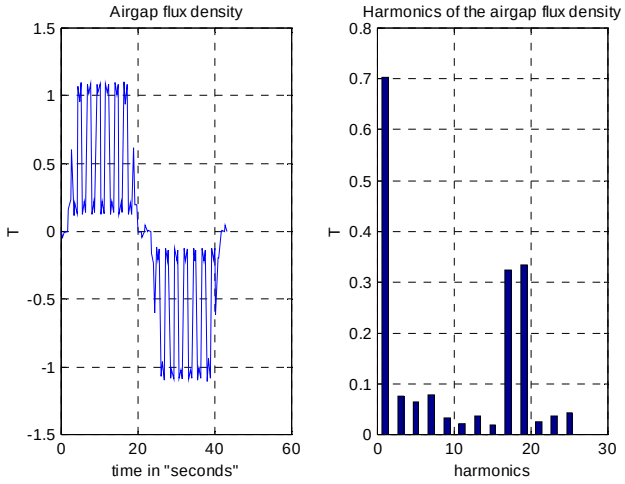

Fig 4: Airgap flux density at a radius R= 105 [mm] with Flux-3D for a non-salient pole machine at no-load.

B. Load airgap flux density

The airgap flux density at nominal load is also analyzed for the non-salient pole machine with the 3D program. The machine was loaded only with the q-component of the current and with the magnet set under phase a. The resulting value of the airgap flux density in these operating conditions is calculated as $\hat{B}_{\delta}$ = 0.69 [T]. The airgap flux density calculated with the 3D program at the center of the machine is shown in Figure 5.

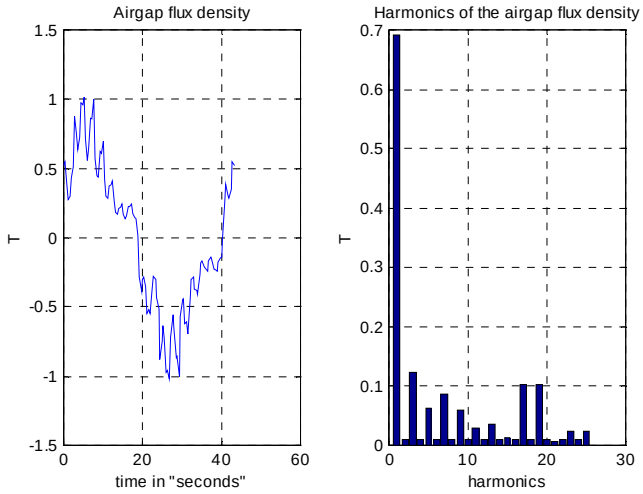

Fig 5: Airgap flux density at a radius R= 105 [mm] with Flux-3D for a non-salient pole machine at rated load.

C. Induced phase voltage calculation

In order to calculate the induced phase voltage, the peak value of the flux linkage produced by the magnet at no load has been calculated. The magnets have been set in such a position that all the flux produced by the magnet passes entirely through phase a, which is placed in the q-direction. The peak value of the flux produced by the magnet, $\hat{\psi}_m$, is found by integrating the stator back flux in the q-direction and corresponds to the flux linked to phase a, that is $\hat{\psi}_m \cong \hat{\psi}_q \cong \hat{\psi}_a$ = 0.1148 [Wb]. The peak value of the induced voltage is then calculated as $\hat{e} = \omega_s \hat{\psi}_m$ = 144.3 [V], which is about 2.7 % lower than the analytical calculations.

D. Synchronous inductance

As a non-salient pole Torus machine is being analyzed, the inductance in the d-direction coincides with the synchronous inductance. Moreover, the machine is fed with a current consisting only of the d-component, which is equal to $\hat{I}_d = \hat{I}_s$ = 131.8[A]. The q-component of the flux is almost zero while the component of the flux in d-direction is $\hat{\psi}_{d.arm}$ = 0.049 [Wb]. The value of the inductance in the d-direction is therefore L_d= 0.372 [mH], which is 13 % higher than the value obtained with the analytical calculations.

E. Cogging Torque

The cogging torque computation was performed with the 3D program. The program automatically calculates the cogging torque as a result of the analysis of subsequent magnetostatic positions of a moving part i.e. the rotor, the magnet and half of the airgap. The results of the calculations of the cogging torque vary depending on the type and thickness of the mesh, which has been applied to the airgap and the different regions. The value of the peak cogging torque obtained in this way varies from 1.1 [Nm] to 2 [Nm].

5. Thermal model

A model of the heat distribution in the machine was discussed and a simplified thermal model was studied. In order to study the thermal model of the machine, several simplifications have been made. First, the heat is assumed to transfer inside the machine along different paths and each material is assumed to have a constant heat conductance and heat capacitance in these regions. Besides this, steady state conditions were analyzed. This implies that the effect of the capacitance was disregarded in this model. In addition, the only thermal sources in the machine are assumed to be the iron losses and the copper losses, which are mainly restricted to the conduction losses, as the presence of stator teeth reduces the eddy currents in the conductors. Consequently the mechanical losses were disregarded. The heat produced in the machine is transferred to the water-cooling system while the heat transferred to the surrounding air is assumed to be negligible. Due to the high conductivity of copper, the heat distribution is assumed to be uniform inside the slot. Thus, the temperature inside each slot can be considered as constant. As the highest current loading occurs at the machine inner part, the temperature is expected to be more elevated in this region. Thus, the heat in the inner part of the teeth will be higher than in the outer part. However, an average temperature can be considered and the thermal analysis can be performed at the middle radius i.e. R = 105 [mm].

6. Experimental Results

The measurements on the machine have been performed on the non-salient pole machine.

A. Induced Voltages

In order to measure the phase-induced voltage, a DC motor has been used to drive the Torus machine. The DC motor has been run at different speeds with the Torus machine at no-load conditions.

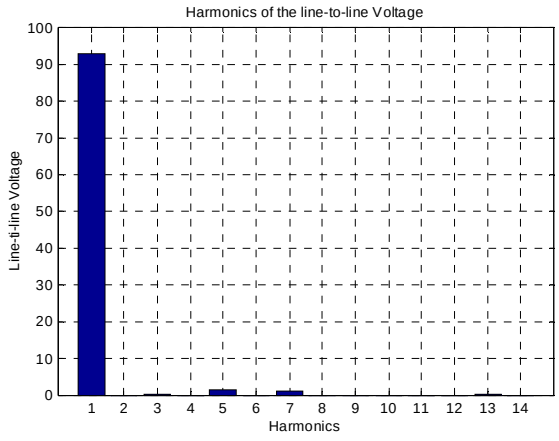

Fig 6: Line-to-line Voltage harmonic spectrum at 2000 [rpm].

A digital power meter has been connected to the stator windings. Figure 6 shows the harmonic content present in the line-to-line voltage at 2000 [rpm].

The value of the analytically calculated line-to-line voltage at 20°C is slightly higher than the measured value at the same temperature. This difference varies between 1.5% at 4000 [rpm] and 0.6% at 1000 [rpm].

B. Inductance in the d-direction

As the machine does not initially possess any saliency, only the inductance in the d-direction, corresponding to the synchronous inductance, is measured. In order to measure the machine inductance in the d-direction a step voltage has been applied to the machine with the rotor locked. The single-phase circuit of the machine in this operating condition is shown in Figure 7.

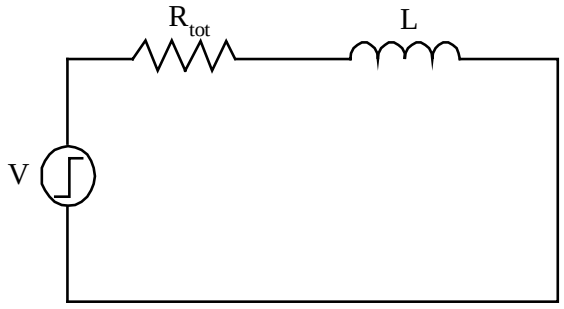

Fig 7: Machine one-phase representation with the rotor locked.

The resistance R_{tot} accounts for different resistances i.e. the single phase resistance of the motor R= 0.022 [Ω], the wire resistance and an external high power resistance R_{ext} = 0.1 [Ω], which has been set in series in the circuit in order to dissipate the power produced when the power supply is switched on. The wire resistance has been evaluated as R_w= 0.02 [Ω]. The inductance L accounts for the main inductance in the d-direction and for the slot leakage inductance.

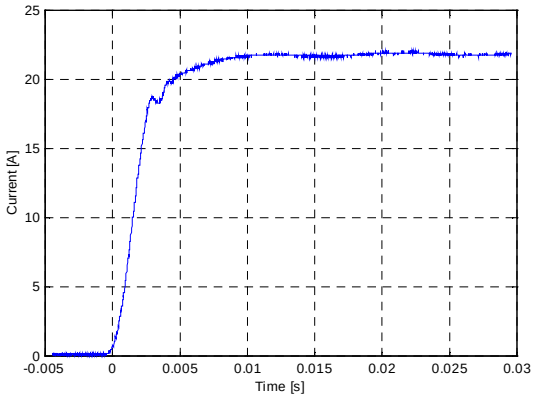

Fig 8: Current variation at the switching of the voltage supply.

From the ratio between the applied step voltage and the slope describing the initial current variation (Figure 8), the value of the total inductance is calculated as L=0.375 [mH]. The value of the slot leakage inductance was calculated as L_{slot}= 8.1 [μH], resulting in a value of the measured inductance in the d-direction L_d = 0.3589

[mH]. The calculated value of the inductance with the analytical calculation was L_d = 0.33 [mH] while the value calculated with the 3D program was 0.372 [mH]. Thus, a higher inductance is measured than the analytically calculated one. However, the measured inductance is lower than the inductance resulting from the FEM calculations and a greater similarity between the two values is shown.

C. Torque

The torque measurement was performed with the generator test by loading the machine with a three-phase resistance. If the machine is run at 2000 [rpm] and the torque is assumed to be half of the rated value i.e. T = 35 [Nm], the value of the single phase current is calculated from the equality between the mechanical and the electric power assuming that the efficiency is η =1. The value of the calculated current is I_{rms} = 46.5 [A] and from this value the load resistance can be evaluated.

The digital power meter connected to output of the Torus machine, measured a line-to-line voltage equal to V_{rms} = 87.64 [V], a current equal to I_{rms} = 42.6 [A], a power of P = 6.45 [kW] and a power factor cosφ = 0.999. The difference observed in the measured value of the electric quantities compared with the calculated values is due both to the difficulty in setting the correct value of the load resistance, and to the assumption of η =1.

As the speed of the machine is kept constant at 2000 [rpm], the torque can be roughly calculated as the ratio between the measured output power and the product of the mechanical speed and the efficiency. Thus, if the efficiency is assumed to be unitary, the torque produced in these operating conditions is T ≈ 31 [Nm].

However, the DC machine was connected to a torque-meter, which measured a torque equal to T ≈ 36 [Nm]. The value of the measured torque is roughly 15% higher than the calculated one. A higher measured value of the torque is reasonable as the efficiency of the machine is not unity (at 2000 [rpm] it was calculated to η =0.954). In addition mechanical losses have to be added. An error in the reading of the torque-meter can also influence the accuracy of the measurement.

D. Cogging Torque

A rough measurement of the peak cogging torque was performed with a mechanical set-up. A long metallic rod was placed perpendicular to the machine shaft and fixed on it in the equilibrium position, see Figure 9.

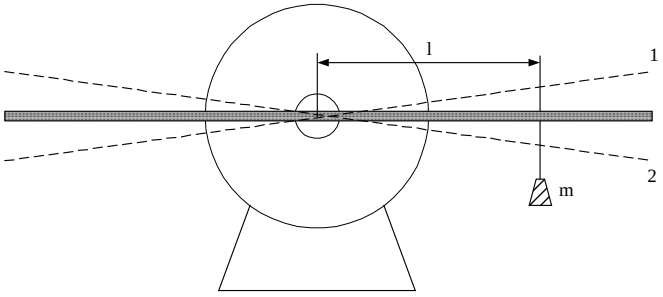

Fig. 9: Set-up for the measurement of the cogging torque [8].

A weight having a mass m equal to m=300 [g] was hung on one side of the rod so as to produce a torque on the shaft. The position of the weight was progressively moved outwards until the torque produced by the weight on the rod caused the rotation of the shaft. The value of the torque produced by the weight in this position corresponds approximately to the peak cogging torque. The same measuring procedure was used on both sides of the rod to take away the effect of the possible asymmetries. Further measurements were performed after moving the rod upwards (position1), downwards (position2) and then in the equilibrium position.

The resulting lowest cogging torque appears when the rod is initially positioned in the direction of rotation of the rotor, which is clockwise in Figure 9. This can be explained as a result of a remanent flux in the teeth, which opposes the movement of the rotor. Using this method, the maximum cogging torque was found to be T_{cog}= 2.8 [Nm].

E. Thermal Test

In order to measure the stator winding temperature, the machine has been run as a generator at different speeds and different current loading until the steady state condition was reached. The value of the average stator temperature was then calculated after having measured the resistance variation after the shut-off of the machine and having extrapolated the resistance value to the shut-off time. Several measurements have been performed in order to measure the temperature of the stator windings and the values of the measured resistances at different operating conditions with the corresponding water flow and water temperature. The curve fitting for the results of these measurements is reported in Figure 10.

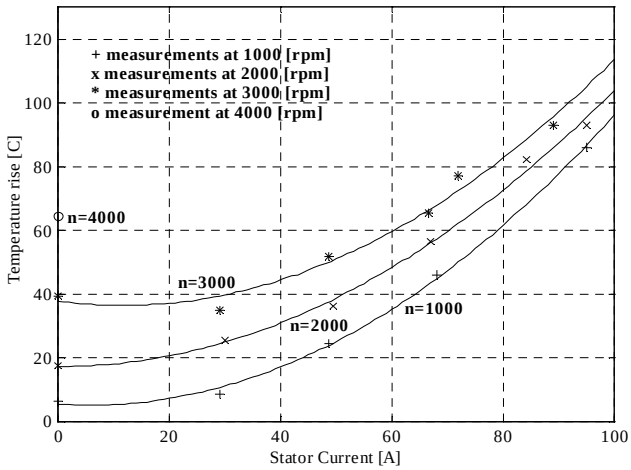

Fig. 10: Temperature rise at different speeds and different current loads.

The measured values of the temperature rise show good agreement with the results of the thermal model at no-load, while higher values are measured than the calculated ones at rated load as shown in Table III.

TABLE III
COMPARISON BETWEEN THE TEMPERATURE RISE OBTAINED WITH THE THERMAL MODEL AND WITH MEASUREMENTS.

Temperature rise		Thermal model [°K]	Measurements [°K]
No load	n=1000 [rpm]	8	6
	n=2000 [rpm]	20	17
	n=3000 [rpm]	39	39
	n=4000 [rpm]	61	64
Rated load	n=1000 [rpm]	73	92
	n=2000 [rpm]	87	101
	n=3000 [rpm]	106	110
	n=4000 [rpm]	138	-

6. Conclusions

This paper has investigated an innovative design of a 30kW, 4000 r/min Torus machine aimed to be integrated inside a drive system for HEVs. In order to render the machine suitable for traction applications, stator teeth have been added to the stator yoke. This results in the improvement of the machine's field-weakening capability. Furthermore, the machine has been designed with rotor saliency in order to further improve its field-weakening range.

After a general overview of the design criteria, which describe the Torus machine parameters, a prototype has been designed. The effect of rotor saliency on the machine has been analytically determined. To this end, the performance of the Torus machine, primarily designed as a salient-pole machine, has been determined for the case where the saliency is removed.

The FEM analysis performed mainly with a 3D software has shown acceptable agreement with the analytical calculations as regards the airgap flux density, the induced phase voltage, the inductance in the d-direction and the cogging torque. The measurements on the machine parameters also validate the analytical results. Unfortunately, the slip of one magnet during the thermal test has hindered the measurements of the machine field-weakening capability. Although a higher discrepancy emerges with varying load, good agreement is shown between the results of the thermal model and the measurements from the thermal test at no-load.

Acknowledgement

The financial support for the work offered by ABB Corporate Research and Swedish National Energy Administration (Energimyndigheten) is gratefully acknowledged.

References

[1] H-N. Lenz, *"Visions for Clean Air - future requirements and developments"* Closing Session of the 18th Int. Electric Vehicle Symposium, EVS 18, on CD, Oct. 2001

[2] D.E. Carlson, *"Fossil Fuels, The greenhouse Effect and Photovoltaic"*, Presentation to the 20th IEEE Photovoltaic Conference, Dec. 1989

[3] A. Di Napoli, F. Caricchi, F. Crescimbini, G. Noia, *"Design criteria of a low-speed axial-flux PM synchronous machine"*, Proc. International Conference on the Evolution and Modern Aspects of Synchronous Machine August 1991

[4] E. Spooner, B.J. Chalmers, "TORUS - a slotless toroidal-stator, permanent-magnet generator", IEE Proc. B, 139, pp. 497-506, November 1992

[5] F. Caricchi, F. Crescimbini, *"Axial-flux permanent magnet machine with water-cooled ironless stator"*, Int. Symp. on Electric Power Eng., Vol.Invited speakers' session, June 1995

[6] Z. Zang, F. Profumo, A. Tenconi, *"Axial flux versus radial flux PM motors"*, Symp. on Power Electronics, Industrial Drives, Power Quality, Traction Systems, June 1996

[7] E. Muljadi, C.P. Butterfield, Yih-huie Wan, *"Axial-Flux Modular Permanent-Magnet Generator with a Toroidal Winding for Wind-Turbine Applications"*, IEEE Transaction on Industry Applications, Vol. 35, No.4, July/August 1999

[8] P. Thelin, *"Integration Aspects and Development of a Compact 15kW PM Integral Motor"*, Technical Licentiate thesis, Royal Institute of Technology, Electrical Machines and Drives, Stockholm 1999